Letter

Universal route to chiral Ising superconductivity in monolayer TaS_2 and $NbSe_2$

Lucia Gibelli,[1] Simon Höcherl,[1] Julian Siegl,[1] Viliam Vaňo,[2] Somesh C. Ganguli,[2] Magdalena Marganska,[3] and Milena Grifoni[1,*]

[1]*Institute for Theoretical Physics, University of Regensburg, 93 053 Regensburg, Germany*

[2]*Department of Applied Physics, Aalto University, FI-00076 Aalto, Finland*

[3]*Department of Theoretical Physics, Wrocław University of Science and Technology, Wybrzeże Wyspiańskiego 27, 50-370 Wrocław, Poland*

(Received 9 September 2025; accepted 24 November 2025; published 29 December 2025)

We investigate Ising superconductivity in two archetypal intrinsic superconductors, monolayer $1H-TaS_2$ and $1H-NbSe_2$, in a bottom-up approach. Using *ab initio*-based tight-binding parametrizations for the relevant low-energy *d* bands, the screened interaction is evaluated microscopically in a scheme including Bloch overlaps. In direct space, the screened potential for both systems displays long-range Friedel oscillations alternating in sign. Upon scaling, the oscillation pattern becomes universal, with the location of minima and maxima locked to the lattice. Solving the momentum-resolved gap equations, a chiral ground state with *p*-like symmetry is generically found. Due to the larger Ising spin-orbit coupling, the chiral gap is more anisotropic in TaS_2 than in $NbSe_2$. This is reflected in tunneling spectra displaying V-shaped features for the former, in quantitative agreement with low-temperature scanning tunneling experiments on TaS_2. At the same time, our results reconcile the apparent discordance with hard gap tunneling spectra reported for the sibling $NbSe_2$.

DOI: 10.1103/bh1n-sc95

Introduction. Few-layer transition metal dichalcogenides (TMDCs) offer unprecedented opportunities to design novel quantum materials by gating and proximity effects with substrates, impurity doping, or by exploiting their strong spin-orbit coupling (SOC). This also concerns their superconducting properties [1].

Among the most investigated intrinsic TMDCs superconductors are $NbSe_2$ and TaS_2, which display charge-density waves already in their bulk phase [2–4] and show signatures of unconventional superconductivity in the few-layer limit [5–8]. The diverse properties of TMDCs are governed by their crystal phases [9]. Here we focus on the trigonal prismatic 1*H*-TMDCs. In their bulk form, these TMDCs possess a global inversion center, but are noncentrosymmetric at the monolayer level. Viewed from above, the monolayer crystal forms a hexagonal lattice similar to graphene but with two inequivalent sublattice sites occupied by the *M* and *X* atoms; see Fig. 1. The lack of inversion symmetry leads to Ising SOC, pinning the electron spins in the out-of-plane direction [1,5,10], which qualitatively impacts key features of the superconducting state. For example, it leads to a violation of the Pauli limit under strong in-plane magnetic fields [1,8,11–16] and yields the potential to realize exotic topological phases [17–19].

Despite recent years having witnessed a surge of growing interest in Ising superconductivity of monolayer TMDCs, the pairing mechanisms are still actively discussed. They range from phonon-mediated [20–22] to more exotic ones resulting from competing electronic repulsion, where even predictions on the symmetry of the gap may differ [19,23–26]. When electron pairing arises from virtual phonon exchange [27], the ions mediate an effective attractive interaction that favors *s*-wave pairing, with gap functions isotropic in momentum space. If superconductivity emerges from screened repulsion, the pairing function is anisotropic [28] and its symmetry is associated to irreducible representations of the crystal. Two-dimensional (2D) systems with triangular lattices allow two-dimensional representations and are potential candidates for becoming chiral superconductors [29–31].

This uncertainty on the nature of superconductivity in few-layer TMDCs is partly due to the inherent difficulty of a realistic modeling of many-body effects, which properly accounts for the reduced screening of the Coulomb interaction in low dimensions [32,33]. Latest *ab initio* studies have confirmed the long-range nature of the screened interaction in monolayer TMDCs [34].

In a recent work [26], some of us proposed a bottom-up approach to unconventional superconductivity in monolayer $NbSe_2$ involving a microscopic calculation of the screened Coulomb interaction. Within a generalized random phase approximation (RPA) in momentum space, a strong suppression of intravalley over intervalley processes due to the electron-hole fluctuations of the metal was demonstrated. In the real space, this gives rise to long-range Friedel oscillations [35] of the screened Coulomb potential alternating in sign. Cooper pairing among the electrons then emerges when taking advantage of the attractive regions, a manifestation of the pure electronic mechanism for superconductivity proposed by Kohn and Luttinger [36]. By solving self-consistent gap equations, the appearance of a chiral ground state with *p*-wave character was found.

Triggered by the above results, some fundamental questions arise which will be investigated in this Letter. The first one concerns the nature of superconductivity in monolayer $1H-TaS_2$, another archetypal TMDC superconductor. Since

*Contact author: Milena.Grifoni@ur.de

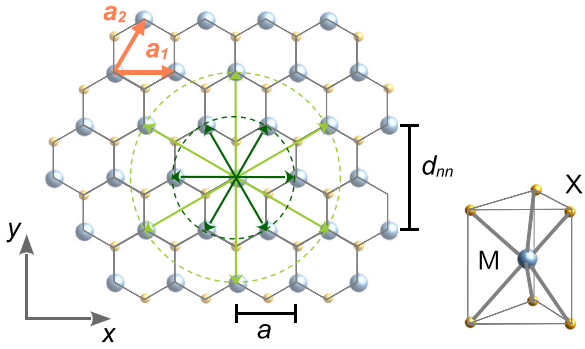

FIG. 1. Crystalline structure of monolayer 1H-TMDCs seen from the top with the metal (blue) and the chalcogen (yellow) atoms. The electronic structure at the Fermi level is mostly determined by the d orbitals of the metal atom. The latter atoms span a triangular lattice with generators $\boldsymbol{a}_1$ and $\boldsymbol{a}_2$. The distance between neighboring metal atoms equals the lattice spacing a in the x direction while $d_{nn} = \sqrt{3}a$ is in the y direction.

the band structure is similar, one can still expect the unconventional Kohn-Luttinger mechanism to apply as for the $NbSe_2$. However, will the stronger Ising SOC [8] also modify the nature of the ground state? If the gap is still chiral, how can one reconcile this with the seemingly different scanning tunneling spectroscopy (STS) spectra reported for the two systems? While low-temperature STS data for $1H-NbSe_2$ are compatible with a fully gapped s-like or chiral phase [37], the STS spectra for $1H-TaS_2$ have rather a V-like shape [38].

In this Letter, we have applied the methodology from Ref. [26] to evaluate the screened interaction in $1H-TaS_2$. To identify universal features, for both test systems the investigation of the real-space interaction was extended to several lattice periods. We found that, upon proper scaling, the Friedel oscillations of $NbSe_2$ and TaS_2 display almost identical behavior, with anisotropic oscillations dictated by the D_{3h} symmetry of the underlying crystalline lattice. In a 2D Fermi liquid, the Kohn-Luttinger anomaly generically leads to p-wave pairing [39]. By solving the gap equations, we confirm the emergence of a p-like chiral ground state also for $1H-TaS_2$. Importantly, the larger Ising SOC arising from the Ta atoms yields a stronger anisotropy of the chiral gap compared to $1H-NbSe_2$. This results in V-shaped tunneling spectra for TaS_2, despite the gapped nature of the chiral phase, similar to the STS experiments [38]. Our results establish the Kohn-Luttinger mechanism as possible route to superconductivity in 2D TMDCs and identify in the distinct strength of the Ising SOC the reason for seemingly different low-temperature STS spectra.

Band structure and orbital composition. We start from a tight-binding model for the Bloch band structure of metallic 1H-TMDCs, like $NbSe_2$ or TaS_2, obtained by using their three most relevant d orbitals [40] fitted to *ab initio* calculations [17,41]; for additional clarity, see also the Supplemental Material (SM) [42] (see also Refs. [43–45] therein). As seen in Fig. 2, there are two metallic bands relevant for superconducting pairing at the Fermi level which are split by Ising SOC [40]. Multiple disjoint Fermi surfaces are present, shown in the insets of Figs. 2(a) and 2(b). While the planar d orbitals mostly contribute to the band composition around the K and K' valleys, $d_{2,0}$ is dominant at the Γ valley [40]. The impact of the Ising SOC is clearly more prominent in TaS_2 than in $NbSe_2$.

We restrict to the spin-split metallic bands at the Fermi level, for which the many-body Hamiltonian in the Bloch

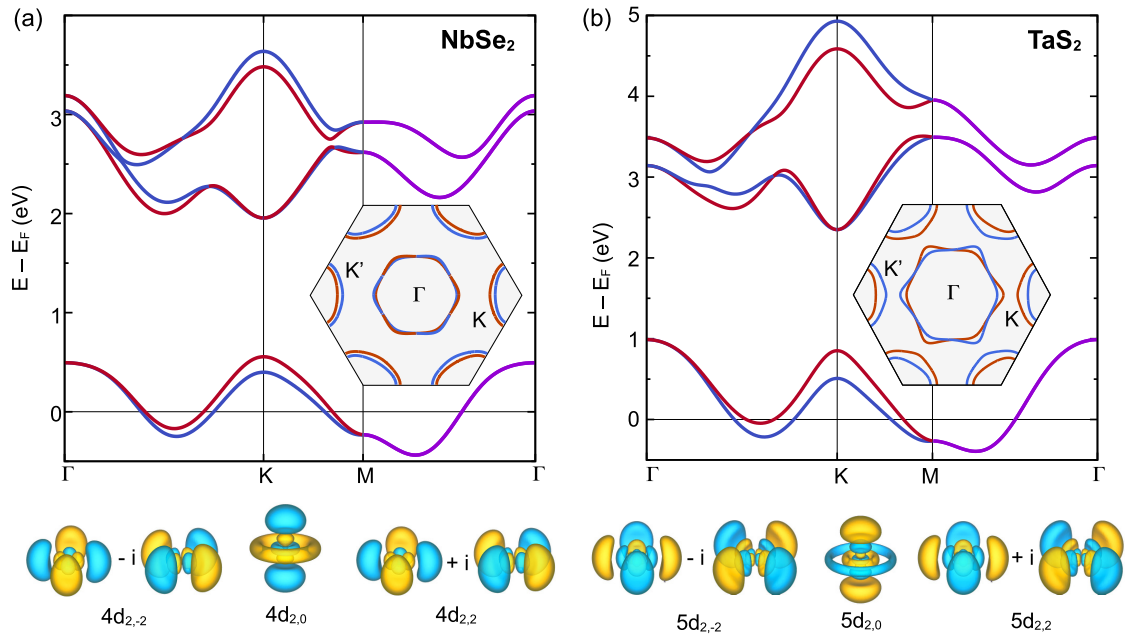

FIG. 2. Band structure, Fermi surface, and orbital contributions in monolayer $1H-NbSe_2$ and $1H-TaS_2$. (a), (b) Tight-binding Bloch bands (top) and Fermi surfaces (inset) with spin degeneracy removed by the Ising spin-orbit coupling. Due to the larger spin-orbit coupling, the Γ- and K-Fermi surfaces get closer in TaS_2 compared to $NbSe_2$. Bottom: Sketch of the three atomic $d_{l,m}$ orbitals used in the calculation. The quantum numbers l, m denote the total angular momentum of the orbital and its azimuthal projection.

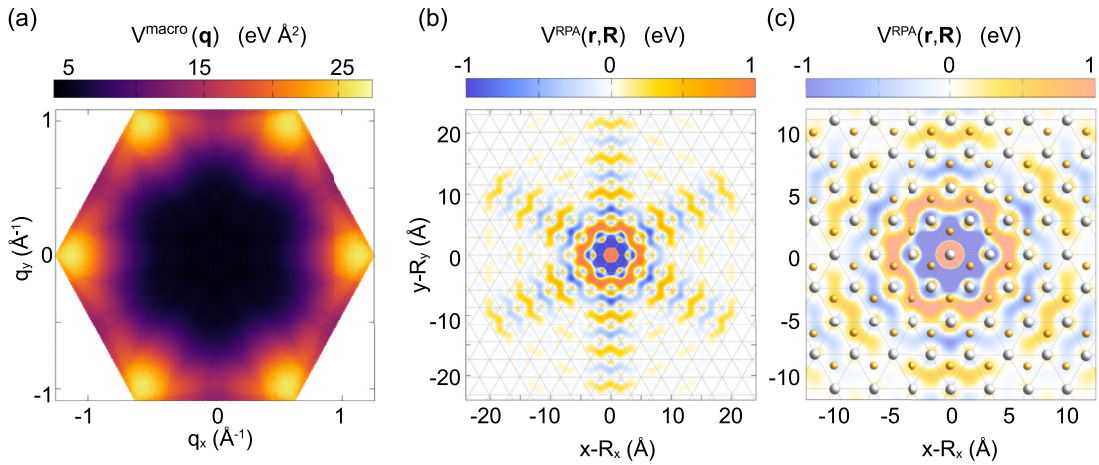

FIG. 3. Screened RPA interaction for TaS_2. (a) In the reciprocal space, the screened interaction is positive and inherits the D_{3h} symmetry of the lattice. The exemplary element of the interaction matrix corresponding to normal processes is shown. It is strongly suppressed at small transferred momenta $\boldsymbol{q}_\Gamma$ while maxima are seen for momenta $\boldsymbol{q}_K$ at the corners of the Brillouin zone. (b) In the real space, the interaction is largely anisotropic and displays Friedel oscillations with alternating positive and negative regions. The oscillations persist longest (shortest) along the y (x) axis (and the lines obtained from those by a $2\pi/6$ rotation). A zoom into the central area of (b) is shown in (c), overlaid with the Ta and S atomic lattice.

basis has the form

$$\hat{H}_{\mathrm{MB}} = \sum_{\boldsymbol{k},\sigma} \xi_{\boldsymbol{k},\sigma} \hat{c}^{\dagger}_{\boldsymbol{k},\sigma} \hat{c}_{\boldsymbol{k},\sigma} + \hat{V}, \tag{1}$$

where the first term describes independent Bloch electrons with energies $\xi_{\boldsymbol{k},\sigma}$ measured from the Fermi level, and $\hat{c}^{(\dagger)}_{\boldsymbol{k},\sigma}$ are annihilation (creation) operators of Bloch electrons with crystal momentum $\boldsymbol{k}$ and spin σ. The second term is the screened Coulomb interaction. Its form is crucial to assess whether a purely electronic pairing mechanism can take place.

Screened Coulomb interaction and Friedel oscillations. In crystalline systems, the screened interaction $V(\boldsymbol{r},\boldsymbol{r}')$ is, in general, a function of both positions of the two interacting charges. A closed form evaluation of the screened interaction can be obtained in the RPA, in which the polarizability is approximated by that of independent Bloch electrons [32]. In monolayer TMDCs, with the d orbitals tightly confined to the plane of the material, one finds the expansion [26]

$$V^{\mathrm{RPA}}(\boldsymbol{r},\boldsymbol{r}') = \frac{1}{\mathcal{A}} \sum_{\boldsymbol{q},\boldsymbol{G},\boldsymbol{G}'} V^{\mathrm{2D}}_{\boldsymbol{G},\boldsymbol{G}'}(\boldsymbol{q}) e^{i(\boldsymbol{q}+\boldsymbol{G})\cdot\boldsymbol{r}} e^{-i(\boldsymbol{q}+\boldsymbol{G}')\cdot\boldsymbol{r}'}, \tag{2}$$

where $\boldsymbol{G}$, $\boldsymbol{G}'$ are reciprocal lattice vectors, $\boldsymbol{q}$ is a crystal momentum, $\mathcal{A}$ is the sample area, and $V^{\mathrm{2D}}_{\boldsymbol{G},\boldsymbol{G}'}(\boldsymbol{q})$ is the screened interaction tensor.

In Fig. 3, we display the screened RPA interaction for TaS_2. The element $V^{\mathrm{macro}}(\boldsymbol{q}) := V^{\mathrm{2D}}_{\boldsymbol{0},\boldsymbol{0}}(\boldsymbol{q})$ is shown in Fig. 3(a) and provides the macroscopic, long-range component of the interaction.

Similarly to what was reported for $NbSe_2$ in Ref. [26], it is strongly suppressed for $\boldsymbol{q} \approx \boldsymbol{q}_\Gamma$, and displays maxima at $\pm\boldsymbol{q}_K$, which supports the scenario of unconventional pairing arising from dominant intervalley scattering [24,46].

When looking at the potential in the real space, $V^{\mathrm{RPA}}(\boldsymbol{r},\boldsymbol{R})$, with $\boldsymbol{r}' = \boldsymbol{R}$ fixed to a Ta site, alternating repulsive and attractive regions are seen, cf. Fig. 3(b). A large anisotropy is observed which respects the D_{3h} symmetry of the lattice with very different decay along preferential directions.

One finds on-site repulsion at the origin and minima or maxima about halfway to neighboring atom sites, Fig. 3(c). Hence, the Friedel oscillations are locked to the lattice, in contrast to the case of the interacting electron gas studied by Kohn and Luttinger for simple metals [36]. We find a very similar oscillation pattern when calculating the screened interaction for $NbSe_2$, which hints at a universal behavior upon proper scaling. This is confirmed in Fig. 4, where the screened interactions for $NbSe_2$ and TaS_2 almost collapse onto the same curve when divided by their value at the origin and plotted in units of the lattice constant. The oscillations persist at very long distances, whereby the longer lasting ones along the y axis are periodic with the next neighbor distance $d_{nn} = \sqrt{3}a$, and the faster decaying ones along the x axis have the period $3a$. This general behavior suggests that the two materials should also share similar features in the superconducting state.

Gap equation and leading instabilities near T_c. We next discuss the properties of the superconducting instability mediated by the screened potential. With this aim, we conveniently work in the Bloch basis. Time-reversal symmetry favors scattering between time-reversal partners, as shown in the SM [42]. We hence consider in the following the interaction matrix elements $V_{\boldsymbol{k},\boldsymbol{k}',\sigma} := \langle \boldsymbol{k}',\sigma;\bar{\boldsymbol{k}}',\bar{\sigma}|\,\hat{V}\,|\boldsymbol{k},\sigma;\bar{\boldsymbol{k}},\bar{\sigma}\rangle$, where $\boldsymbol{k},\boldsymbol{k}'$ are in-plane momenta within the first Brillouin zone. The restriction to Kramers pairs of Bloch states yields a low-energy Hamiltonian of the typical BCS form [27]. Performing a mean field approximation, in turn, leads to the familiar BCS gap equation

$$\Delta_{\boldsymbol{k},\sigma} = -\sum_{\boldsymbol{k}'} V_{\boldsymbol{k},\boldsymbol{k}',\sigma} \Pi(E_{\boldsymbol{k}',\sigma}) \Delta_{\boldsymbol{k}',\sigma}, \tag{3}$$

where the gap enters $\Pi(E) = \tanh(\beta E/2)/2E$ through the quasiparticle energies $E_{\boldsymbol{k},\sigma} = \sqrt{\xi^2_{\boldsymbol{k},\sigma} + |\Delta_{\boldsymbol{k},\sigma}|^2}$, and $\beta = 1/k_B T$ is the inverse temperature.

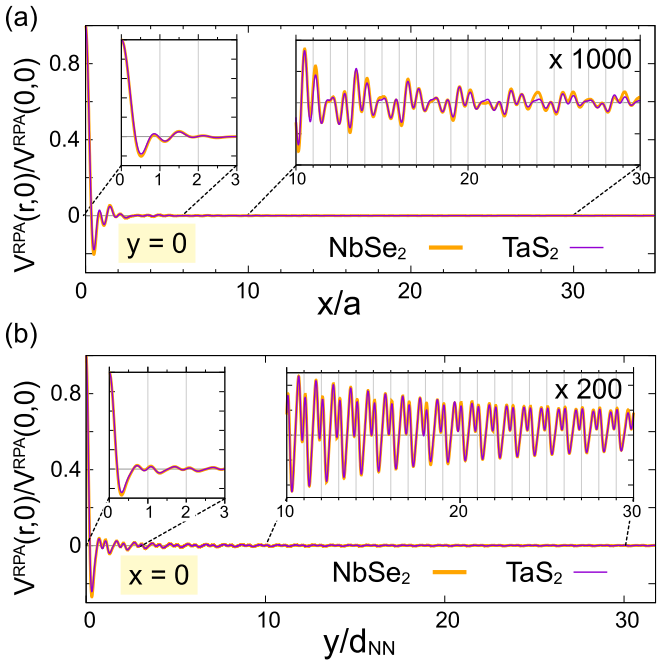

FIG. 4. Universality of Friedel oscillations. The screened potentials for TaS_2 and $NbSe_2$ almost collapse onto the same curve when scaled by their value at the origin and plotted in units of the respective lattice constant. The oscillations persist over long distances and have a periodicity $3a$ in the x direction and $d_{nn} = \sqrt{3}a$ in the y direction. The lattice spacings are taken to be $a_{TaS_2} = 3.342$ Å, $a_{NbSe_2} = 3.445$ Å; the interactions $V^{RPA}_{TaS_2}(0,0) = 24.33$ eV, $V^{RPA}_{NbSe_2}(0,0) = 23.07$ eV.

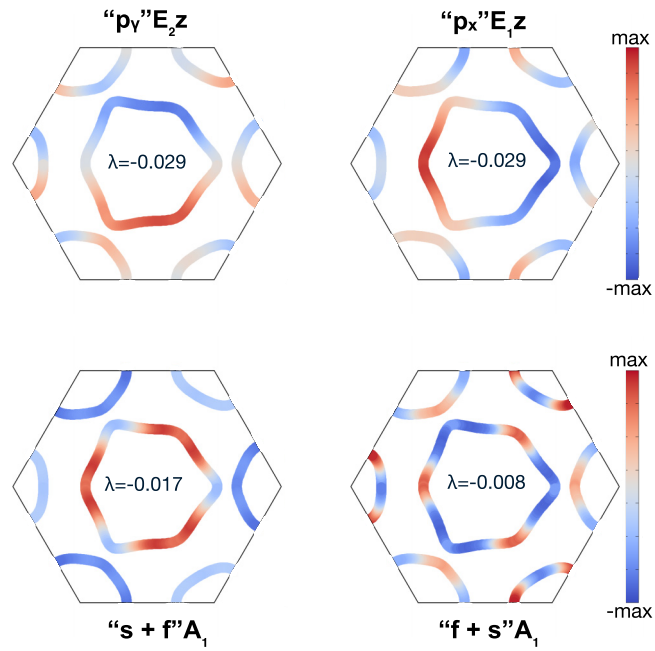

FIG. 5. Instabilities near T_c for TaS_2. At the critical temperature, the leading gaps are twofold degenerate solutions of predominant E' z-triplet type (top panels). They are followed by SOC-allowed linear combinations of the A_1' type (bottom panels). Due to the strong admixture of s-like and f-like contributions, these gaps have nodes on the Γ Fermi surfaces. A complex linear combination of the nematic E' solutions results in a fully gapped chiral gap.

To access observables near the phase transition, one linearizes Eq. (3) by replacing the excitation energies $E_{\boldsymbol{k},\sigma}$ with the single-particle energies $\xi_{\boldsymbol{k},\sigma}$ and solving the resulting linear problem in a range of $\pm\Lambda$ around the Fermi energy [19,25]. The instabilities with the highest T_c for $NbSe_2$ have been investigated in Ref. [25] using a top-down Hubbard-Kanamori model in the atomic basis and in Ref. [26] within the bottom-up approach also adopted in this Letter. Here we focus on the leading instabilities of $1H - TaS_2$, which are shown in Fig. 5. They belong to irreducible representations of the D_{3h} symmetry group. We find as the dominant pairing two degenerate nematic p-like solutions of the E' z-triplet type (with singlet admixture). Similar conclusions have been reported in a top-down model calculation by Roy *et al.* [47]. These solutions are followed by the SOC-introduced combinations of the A_1' s-like singlet and f-like z triplet, with the latter a previously discussed candidate for the superconducting phase of monolayer TaS_2 [38]. The critical temperatures of these solutions depend on the associated eigenvalues λ of the pairing matrix and the cutoff in energy which we fixed to $\Lambda = 100$ meV.

Chiral $p_x + ip_y$ groundstate and comparison with experiments. The two leading solutions of the pristine system are degenerate nematic gaps, which will remain quasidegenerate for weak enough breaking of the symmetry. This allows for the emergence of a chiral gap, i.e., a complex linear combination of the two nematic solutions, at temperatures below T_c [48]. To what extent a nodal nematic solution or the gapped chiral phase is the preferred ground state can be determined by solving the self-consistency equation, Eq. (3), as a function of temperature. To this aim, we expanded both the interaction and the order parameter in basis functions of the appropriate irreducible representations of the D_{3h} symmetry group [19,49,50] and solved a set of coupled equations for the expansion coefficients as a function of the temperature. We find a fully gapped chiral phase at zero temperature, similarly to what was predicted for monolayer $NbSe_2$ [26]. The magnitude of this chiral gap at $T = 0$ mK is displayed in Fig. 6 together with a comparison with the experimental STS data from Ref. [38]. As seen in Fig. 6(a), the chiral gap is strongly dispersive on the Γ Fermi surface, where it also attains its maximal value. The experiments were performed on monolayer $1H - TaS_2$ epitaxially grown on a highly oriented pyrolitic graphite substrate; see Ref. [38] for details of the setup. The measured observable is the differential tunneling conductance (dI/dV), which is proportional to the spectral function of the sample. The experimental dI/dV averaged over 12 spectra measured at different locations at 350 mK is shown in Fig. 6(b) and fitted to the tunneling density of states obtained from the chiral gap. The theoretical differential conductance shown in Fig. 6(b) is calculated using the coupling to the Γ and K Fermi pockets as free parameters. A table of the used parameters is found in the SM [42]. We find a much larger coupling to the states on the Γ Fermi surface compared to those near the K and K' valleys, in agreement with the sensitivity of STM to states with small in-plane momentum [45,51], and the $d_{2,0}$ character of the

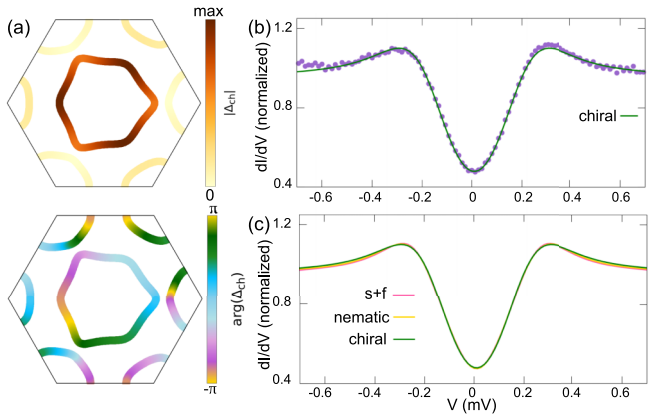

FIG. 6. Chiral gap and STS spectra for TaS_2. (a) A complex linear combination of the two E' z triplets provides the ground state of the system. It is fully gapped with a phase winding clockwise around the Γ Fermi surface. (b), (c) Experimental spectra recorded at $T = 350$ mK are well fitted with a theoretically evaluated differential conductance which uses the chiral gap. A similar good agreement is found if the nematic or the $s + f$ solutions are used since the associated best fit theoretical curves are very close.

orbitals at the Γ valley. Despite the quasiparticle spectrum being fully gapped, the strong variation of the order parameter on the Γ Fermi surface leads to tunneling spectra mimicking a nodal gap, i.e., a V-like shape of the dI/dV as observed in the experiment. Indeed, the same spectroscopy data could be fitted by assuming a standard nodal f gap [38]. By using the nematic solution or the subleading $s + f$ gap function, a similar good fit can be obtained as well, as seen in Fig. 6(c).

Conclusions. Our results show that a mechanism purely based on long-range screened Coulomb repulsion can reconcile theoretical expectations of chiral superconductivity in 2D triangular lattices with seemingly contradicting low-temperature STS experiments. To this extent, it is crucial to account for the Ising SOC present in the monolayer TMDCs, which mixes nominally even and odd solutions and yields a dispersive, albeit gapped, chiral phase. Despite the above results being promising, they are not yet conclusive: Further experiments are needed to confirm the chiral nature of the gap, while a full theoretical treatment should include electron- and phonon-mediated mechanisms on the same footing.

While the focus of this Letter was on intrinsic TMDCs superconductors, the bottom-up method developed here is more general and could be helpful to unravel universal features and the leading pairing mechanism of other low-dimensional superconductors. A natural candidate is monolayer MoS_2, a direct gap semiconductor which becomes superconducting upon doping [52] and for which a Kohn-Luttinger mechanism has been suggested [46]. Furthermore, evidence for chiral d-wave superconductivity has been reported for tin monolayers on a Si(111) surface [53], and a transition from a nematic to a chiral phase has been proposed for the layered $4Hb - TaS_2$ [54,55].

Acknowledgments. Funding was provided by the CRC 1277 and RTG 2905 - 502572516 of the Deutsche-Forschungsgemeinschaft. The experiments made use of the Aalto Nanomicroscopy Center (Aalto NMC) facilities with support from the Academy of Finland (Academy Research Fellow No. 361420).

Data availability. The data that support the findings of this article are openly available [56].

[1] D. Zhang and J. Falson, Ising pairing in atomically thin superconductors, Nanotechnology **32**, 502003 (2021).
[2] J. Wilson, F. Di Salvo, and S. Mahajan, Charge-density waves and superlattices in the metallic layered transition metal dichalcogenides, Adv. Phys. **24**, 117 (1975).
[3] S. Nagata, T. Aochi, T. Abe, S. Ebisu, T. Hagino, Y. Seki, and K. Tsutsumi, Superconductivity in the layered compound 2H-TaS_2, J. Phys. Chem. Solids **53**, 1259 (1992).
[4] A. Sanna, C. Pellegrini, E. Liebhaber, K. Rossnagel, K. J. Franke, and E. K. U. Gross, Real-Space anisotropy of the superconducting gap in the charge-density wave material 2H-$NbSe_2$, npj Quantum Mater. **7**, 6 (2022).
[5] X. Xi, Z. Wang, W. Zhao, J.-H. Park, K. T. Law, H. Berger, L. Forró, J. Shan, and K. F. Mak, Ising pairing in superconducting $NbSe_2$ atomic layers, Nat. Phys. **12**, 139 (2016).
[6] Y. Xing, K. Zhao, P. Shan, F. Zheng, Y. Zhang, H. Fu, Y. Liu, M. Tian, C. Xi, H. Liu, J. Feng, X. Lin, S. Ji, X. Chen, Q.-K. Xue, and J. Wang, Ising superconductivity and quantum phase transition in macro-size monolayer $NbSe_2$, Nano Lett. **17**, 6802 (2017).
[7] E. Navarro-Moratalla, J. O. Island, S. Mañas-Valero, E. Pinilla-Cienfuegos, A. Castellanos-Gomez, J. Quereda, G. Rubio-Bollinger, L. Chirolli, J. A. Silva-Guillén, N. Agraït, G. A. Steele, F. Guinea, H. S. J. van der Zant, and E. Coronado, Enhanced superconductivity in atomically thin TaS_2, Nat. Commun. **7**, 11043 (2016).
[8] S. C. de la Barrera, M. R. Sinko, D. P. Gopalan, N. Sivadas, K.L. Seyler, K. Watanabe, T. Taniguchi, A. W. Tsen, X. Xu, D. Xiao, and B. M. Hunt, Tuning Ising superconductivity with layer and spin–orbit coupling in two-dimensional transition-metal dichalcogenides, Nat. Commun. **9**, 1427 (2018).
[9] M. Chhowalla, H. S. Shin, G. Eda, L.-J. Li, K. P. Loh, and H. Zhang, The chemistry of two-dimensional layered transition metal dichalcogenide nanosheets, Nat. Chem **5**, 263 (2013).
[10] X. Xu, W. Yao, D. Xiao, and T. F. Heinz, Spin and pseudospins in layered transition metal dichalcogenides, Nat. Phys. **10**, 343 (2014).
[11] P. A. Frigeri, D. F. Agterberg, A. Koga, and M. Sigrist, Superconductivity without inversion symmetry: MnSi versus $CePt_3Si$, Phys. Rev. Lett. **92**, 097001 (2004).
[12] X. Xi, H. Berger, L. Forró, J. Shan, and K. F. Mak, Gate tuning of electronic phase transitions in two-dimensional $NbSe_2$, Phys. Rev. Lett. **117**, 106801 (2016).
[13] S. Ilić, J. S. Meyer, and M. Houzet, Enhancement of the upper critical field in disordered transition metal dichalcogenide monolayers, Phys. Rev. Lett. **119**, 117001 (2017).

[14] D. Möckli and M. Khodas, Magnetic-field induced $s + if$ pairing in Ising superconductors, Phys. Rev. B **99**, 180505(R) (2019).

[15] C. W. Cho, J. Lyu, L. An, T. Han, K. T. Lo, C. Y. Ng, J. Hu, Y. Gao, G. Li, M. Huang, N. Wang, J. Schmalian, and R. Lortz, Nodal and nematic superconducting phases in $NbSe_2$ monolayers from competing superconducting channels, Phys. Rev. Lett. **129**, 087002 (2022).

[16] L. Engström, L. Zullo, T. Cren, A. Mesaros, and P. Simon, Upper critical field and pairing symmetry of Ising superconductors, Phys. Rev. Lett. **135**, 236004 (2025).

[17] W.-Y. He, B. T. Zhou, J. J. He, N. F. Q. Yuan, T. Zhang, and K. T. Law, Magnetic field driven nodal topological superconductivity in monolayer transition metal dichalcogenides, Commun. Phys. **1**, 40 (2018).

[18] W. Chen, Q. Zhu, and Y. Zhou, Topological Ising pairing states in monolayer and trilayer TaS_2, Phys. Rev. B **100**, 054503 (2019).

[19] D. Shaffer, J. Kang, F. J. Burnell, and R. M. Fernandes, Crystalline nodal topological superconductivity and Bogolyubov Fermi surfaces in monolayer $NbSe_2$, Phys. Rev. B **101**, 224503 (2020).

[20] N. F. Hinsche and K. S. Thygesen, Electron–Phonon interaction and transport properties of metallic bulk and monolayer transition metal dichalcogenide TaS_2, 2D Mater. **5**, 015009 (2017).

[21] F. Zheng and J. Feng, Electron-phonon coupling and the coexistence of superconductivity and charge-density wave in monolayer $NbSe_2$, Phys. Rev. B **99**, 161119(R) (2019).

[22] S. Das, H. Paudyal, E. R. Margine, D. F. Agterberg, and I. I. Mazin, Electron-phonon coupling and spin fluctuations in the Ising superconductor $NbSe_2$, Npj Comput. Mater. **9**, 66 (2023).

[23] D. Wickramaratne, S. Khmelevskyi, D. F. Agterberg, and I. I. Mazin, Ising superconductivity and magnetism in $NbSe_2$, Phys. Rev. X **10**, 041003 (2020).

[24] S. Hörhold, J. Graf, M. Marganska, and M. Grifoni, Two-bands Ising superconductivity from Coulomb interactions in monolayer $NbSe_2$, 2D Mater. **10**, 025008 (2023).

[25] S. Roy, A. Kreisel, B. M. Andersen, and S. Mukherjee, Unconventional pairing in Ising superconductors: Application to monolayer $NbSe_2$, 2D Mater. **12**, 015004 (2025).

[26] J. Siegl, A. Bleibaum, W. Wan, M. Kurpas, J. Schliemann, M. M. Ugeda, M. Marganska, and M. Grifoni, Friedel oscillations and chiral superconductivity in monolayer $NbSe_2$, Nat. Commun. **16**, 8228 (2025).

[27] J. Bardeen, L. N. Cooper, and J. R. Schrieffer, Theory of superconductivity, Phys. Rev. **108**, 1175 (1957).

[28] D. J. Scalapino, A common thread: The pairing interaction for unconventional superconductors, Rev. Mod. Phys. **84**, 1383 (2012).

[29] A. P. Mackenzie, T. Scaffidi, C. W. Hicks, and Y. Maeno, Even odder after twenty-three years: The superconducting order parameter puzzle of Sr_2RuO_4, npj Quantum Mater. **2**, 40 (2017).

[30] A. M. Black-Schaffer and C. Honerkamp, Chiral d-wave superconductivity in doped graphene, J. Phys.: Condens. Matter **26**, 423201 (2014).

[31] R. Nandkishore, L. S. Levitov, and A. V. Chubukov, Chiral superconductivity from repulsive interactions in doped graphene, Nat. Phys. **8**, 158 (2012).

[32] M. S. Hybertsen and S. G. Louie, Electron correlation in semiconductors and insulators: Band gaps and quasiparticle energies, Phys. Rev. B **34**, 5390 (1986).

[33] M. Rohlfing and S. G. Louie, Electron-Hole excitations and optical spectra from first principles, Phys. Rev. B **62**, 4927 (2000).

[34] H. R. Ramezani, E. Şaşıoğlu, H. Hadipour, H. R. Soleimani, C. Friedrich, S. Blügel, and I. Mertig, Nonconventional screening of Coulomb interaction in two-dimensional semiconductors and metals: A comprehensive constrained random phase approximation study of MX_2(M = Mo, W, Nb, Ta; X=S, Se, Te), Phys. Rev. B **109**, 125108 (2024).

[35] J. Friedel, XIV. The distribution of electrons round impurities in monovalent metals, London Edinburgh Philos. Mag. J. Sci. **43**, 153 (1952).

[36] W. Kohn and J. M. Luttinger, New mechanism for superconductivity, Phys. Rev. Lett. **15**, 524 (1965).

[37] W. Wan, P. Dreher, D. Muñoz-Segovia, R. Harsh, H. Guo, A. J. Martínez-Galera, F. Guinea, F. de Juan, and M. M. Ugeda, Observation of superconducting collective modes from competing pairing instabilities in single-layer $NbSe_2$, Adv. Mater. **34**, 2206078 (2022).

[38] V. Vaňo, S. C. Ganguli, M. Amini, L. Yan, M. Khosravian, G. Chen, S. Kezilebieke, J. L. Lado, and P. Liljeroth, Evidence of nodal superconductivity in monolayer 1H-TaS_2 with hidden order fluctuations, Adv. Mater. **35**, 2305409 (2023).

[39] A. V. Chubukov, Kohn-Luttinger effect and the instability of a two-dimensional repulsive Fermi liquid at T = 0, Phys. Rev. B **48**, 1097 (1993).

[40] G.-B. Liu, W.-Y. Shan, Y. Yao, W. Yao, and D. Xiao, Three-band tight-binding model for monolayers of group-VIB transition metal dichalcogenides, Phys. Rev. B **88**, 085433 (2013).

[41] G. Margalit, E. Berg, and Y. Oreg, Theory of multi-orbital topological superconductivity in transition metal dichalcogenides, Ann. Phys. **435**, 168561 (2021), Special Issue on Philip W. Anderson.

[42] See Supplemental Material at http://link.aps.org/supplemental/10.1103/bh1n-sc95 for details of the tight-binding parametrization, matrix elements of the screened interaction, experimental setup and methods, comparison to STS data, and fit parameters for the superconducting gaps.

[43] E. Clementi, D. L. Raimondi, and W. P. Reinhardt, Atomic screening constants from SCF functions. II. Atoms with 37 to 86 Electrons, J. Chem. Phys. **47**, 1300 (1967).

[44] S. Kim and Y.-W. Son, Quasiparticle energy bands and Fermi surfaces of monolayer $NbSe_2$, Phys. Rev. B **96**, 155439 (2017).

[45] M. M. Ugeda, A. J. Bradley, Y. Zhang, S. Onishi, Y. Chen, W. Ruan, C. Ojeda-Aristizabal, H. Ryu, M. T. Edmonds, H.-Z. Tsai, A. Riss, S.-K. Mo, D. Lee, A. Zettl, Z. Hussain, Z.-X. Shen, and M. F. Crommie, Characterization of collective ground states in single-layer $NbSe_2$, Nat. Phys. **12**, 92 (2016).

[46] R. Roldán, E. Cappelluti, and F. Guinea, Interactions and superconductivity in heavily doped MoS_2, Phys. Rev. B **88**, 054515 (2013).

[47] S. Roy, A. Kreisel, B. M. Andersen, and S. Mukherjee, Unconventional superconductivity in monolayer transition metal dichalcogenides, Phys. Rev. B (2025), doi: 10.1103/6rc6-mm3b.

[48] C. Kallin and J. Berlinsky, Chiral superconductors, Rep. Prog. Phys. **79**, 054502 (2016).

[49] D. Shaffer, F. J. Burnell, and R. M. Fernandes, Weak-Coupling theory of pair density wave instabilities in transition metal dichalcogenides, Phys. Rev. B **107**, 224516 (2023).

[50] J. Haniš, M. Milivojević, and M. Gmitra, Distinguishing nodal and nonunitary superconductivity in quasiparticle interference of an Ising superconductor with Rashba spin-orbit coupling: The example of $NbSe_2$, Phys. Rev. B **110**, 104502 (2024).

[51] J. Tersoff and D. R. Hamann, Theory and application for the scanning tunneling microscope, Phys. Rev. Lett. **50**, 1998 (1983).

[52] J. M. Lu, O. Zheliuk, I. Leermakers, N. F. Q. Yuan, U. Zeitler, K. T. Law, and J. T. Ye, Evidence for two-dimensional Ising superconductivity in gated MoS_2, Science **350**, 1353 (2015).

[53] F. Ming, X. Wu, C. Chen, K. D. Wang, P. Mai, T. A. Maier, J. Strockoz, J. W. F. Venderbos, C. González, J. Ortega, S. Johnston, and H. H. Weitering, Evidence for chiral superconductivity on a silicon surface, Nat. Phys. **19**, 500 (2023).

[54] A. Ribak, R. M. Skiff, M. Mograbi, P. K. Rout, M. H. Fischer, J. Ruhman, K. Chashka, Y. Dagan, and A. Kanigel, Chiral superconductivity in the alternate stacking compound 4Hb-TaS_2, Science **6**, eaax9480 (2020).

[55] I. Silber, S. Mathimalar, I. Mangel, A. Nayak, O. Green, N. Avraham, H. Beidenkopf, I. Feldman, A. Kanigel, A. Klein, M. Goldstein, A. Banerjee, E. Sela, and Y. Dagan, Two-Component nematic superconductivity in 4Hb-TaS_2, Nat. Commun. **15**, 824 (2024).

[56] L. Gibelli, S. Höcherl, J. Siegl, V. Vaňo, S. C. Ganguli, M. Marganska, and M. Grifoni, Data archive of "A universal route to chiral Ising superconductivity in monolayer TaS_2 and $NbSe_2$," Universität Regensburg (2025), http://doi.org/10.5283/epub.77675.